2.5. *pH measurements of tested materials*

The 4 tested materials were manipulated as described in Table 1 and then placed in a mould of 4 mm diameter and 6 mm height.[23,24] The materials were immediately placed in a falcon tube and 5 ml of deionised water were added to the tested materials. pH measurements were recorded using a pH metre (Sartorius PB-11, Melsungen, Germany) at 0, 2, 30, 60 and 1440 minutes after placing the materials in the test tubes.[23,24] Five separate trials were conducted for each material and the means of results were recorded for each material.

3. Results

3.1. *Cytotoxicity evaluation with the transwell insert model results*

Fig. 1 shows the MTT results of tested materials. The largest mean count value to the least mean count value is corresponding to the following materials: 45S5 bioglass paste, Caviton, SuperSeal, and Fuji I glass ionomer cement. There were no significant differences ($p < 0.05$) between the recorded values of the MTT counts for all tested materials.

3.2. *Morphological observation of the cultured pulp cells*

The cultured RPC-C2A cells appeared spindle-shape before confluent; however after confluent the cells became polygonal in shape (Fig. 2A). 45S5 bioglass paste elicited little cytotoxic effects on the morphology of the cultured cells however the size of the cells became slightly smaller in size. The density of the cultured cells decreased in the glass ionomer cement group and then in the Caviton group respectively with marked

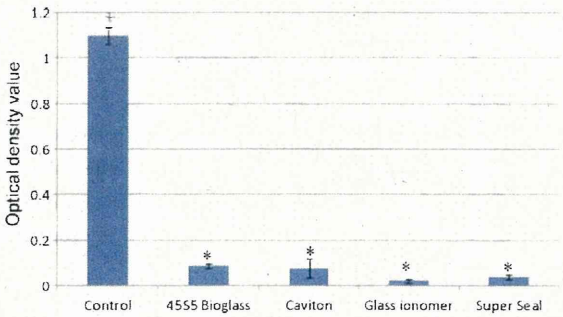

Fig. 1 – Cytotoxicity of four dental materials with culture medium on rat dental pulp cells. MTT results ($n = 5$) of tested materials. One-way ANOVA revealed a significant difference ($p < 0.05$). The same symbols (+, *) represented that there were no significant differences.

increase in the intercellular spaces. Moreover, some of the pulp cells became retracted or rounded, with loss of functional organisation. The SuperSeal group showed marked increase of cell degeneration, cell debris and signs of pulpal cells necrosis.

3.3. *pH measurements of tested materials*

The mean of the pH values are shown in Fig. 3. The initial pH measurements of the 45S5 bioglass mixture were initially acidic i.e. 2.2, however there was a slightly steady increase in the pH along the period of observation till it reached 4 after 24 h. The SuperSeal maintained its acidic behaviour along the experimental period. The glass ionomer and the Caviton showed higher pH values that remained relatively stable throughout the experiment.

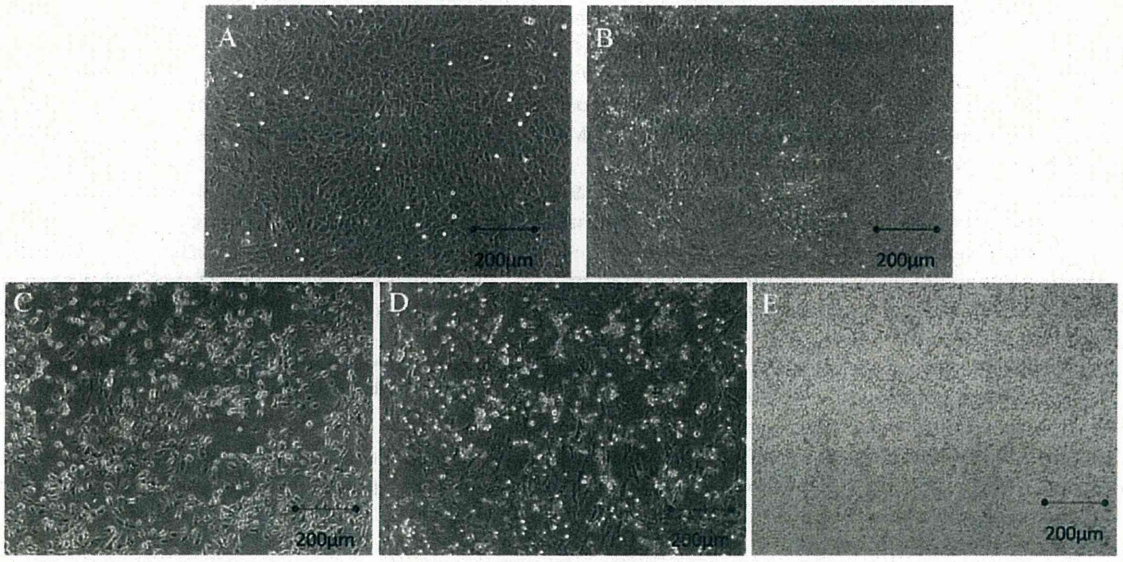

Fig. 2 – Morphological changes of pulp cells following exposure to the various tested materials for 3 days. (A) Control pulp cells: polygonal-shaped cells can be observed and (B) 45S5 bioglass paste group: size of the cells became slightly smaller. (C) Caviton group: decrease in pulp cells density and increase in intercellular spaces. (D) Glass ionomer group: decrease in pulp cells and marked increase in intercellular spaces. (E) SuperSeal group: marked observation of cell degeneration, cell debris and signs of pulpal cells necrosis (100×, original magnification).

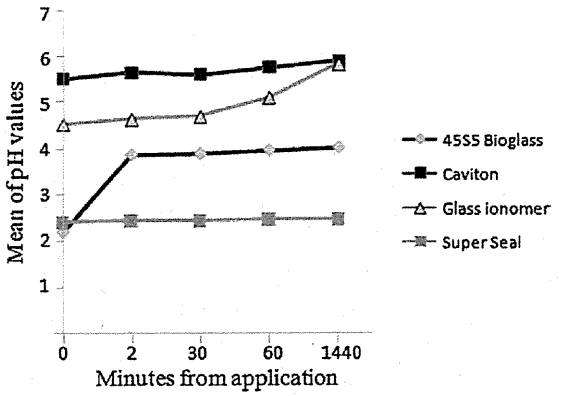

Fig. 3 – Mean of the pH values recorded for the tested materials at the experimental durations.

4. Discussion

45S5 bioglass is a highly biocompatible material[25] that has an antibacterial effect.[26,27] It was previously reported that the combination of 45S5 bioglass with phosphoric acid will form a calcium phosphate rich layer that can bond to dentine.[19] Moreover, this layer showed good abrasion resistance and acceptable mechanical properties.[20]

The viability of the cells observed by the MTT experiment showed that the 45S5 bioglass paste did not exert any significant cytotoxic effects on the cultured pulp cells when compared to the results obtained from the other tested commercially available materials. Moreover, 45S5 bioglass showed the least cytotoxic effects on the morphology of the cultured cells when observed under the microscope.

The slight difference between the MTT experiment results and the microscopic examination results may be attributed to the low metabolic activity of the cultured cells caused by the application of the dental materials which may have caused difficulty in obtaining significant differences in the MTT counts when comparing the tested materials.[28]

The highest cytotoxicity was associated with the SuperSeal which is mainly composed of oxalic acid and potassium salts with pH 2.7. This acidic solution depends on attacking the peritubular dentine and using the dentine's calcium to form insoluble calcium oxalate crystals capable of blocking the dentinal tubules orifices.[29] Thus, it is speculated that this solution caused the drop of the pH of the culture media which had a negative effect on the cultured cells.

On the other hand, there were some cytotoxic effects associated with the 45S5 bioglass paste because it is initially acidic after mixing (i.e. pH 2.2) however, due to the rich calcium and phosphate contents of the powder the pH of the paste was gradually increasing to be 4 after 24 h. Thus it is expected that the bioglass mixture exhibited some cytotoxic effects on the cells initially after mixing due to its initial acidity, however these effects were rapidly diminished. It was suggested that the mechanism of calcium-phosphate crystals formation by the 45S5 bioglass paste on tooth surfaces using our technique is as follows: when the 45S5 bioglass powder was mixed with the aqueous solution of the 50% phosphoric acid the calcium, phosphate and sodium crystals leached into the aqueous acidic media.[19,20,30] The phosphate ions released from 45S5 bioglass and those abundant in the phosphoric acid solution reacted with the calcium ions from bioglass and dentine to form calcium-phosphate salts. These inorganic salts precipitated on top of the dentinal-surface with smaller crystals penetrating the dentinal-tubules.[19,20]

There were some cytotoxic effects observed for the glass ionomer group and the Caviton group which may be attributed to the leaching of some cytotoxic components from these materials. In case of glass ionomer it is speculated that some unreacted polyacrylic acid[31] might have permeated from the cellulose acetate filter of the transwell and affected the viability of the cultured cells. The cytotoxic effects observed in the Caviton group may be attributed to its calcium sulphate content which was previously reported to exhibit a moderate cytotoxic effect on the pulp cells.[32]

This in vitro cytotoxicity testing may offer some advantages when compared to in vivo testing as it is rather quick to perform, less expensive, able to be standardised, able to provide large-scale screening and more sensitive method for detecting any slight negative effects on the pulp cells.[33] However, the In vivo studies using animals permit the analysis of biocompatibility under conditions that allow for cell-to-cell interactions that more closely mimic the clinical situation.[34]

However, conducting a direct correlation between the results obtained from the current study to corresponding results derived from in vivo study or any clinical trial should be cautioned against, because in the clinical situation it is expected to place these tested materials on dentine which will act as barrier between the dental materials and the pulp cells, this dentine barrier can alleviate the cytotoxicity of many dental materials and acts as a good pH buffering structure.[35]

Moreover, the dentinal fluid and proteins present within dentinal tubules are able to effectively neutralize the toxic effects of many components released from a variety of restorative dental materials.[36] Thus, it is expected that the current tested materials will exhibit better biocompatibility to the dental pulp cells clinically.

The durability of using the 45S5 bioglass[20] paste and its high biocompatibility suggest that this paste can serve as an efficient aid in the treatment of dentine hypersensitivity.

5. Conclusion

The 45S5 paste showed good biocompatibility to pulp cells when compared to three commercially available dental materials suggesting the safety of using this paste as an aid in treatment of dentine hypersensitivity.

Acknowledgements

This study was supported by grant in aid from JSPS and the GCOE Program, ICTB at TMDU.

REFERENCES

1. Orchardson R, Gillam DG. Managing dentin hypersensitivity. *Journal of the American Dental Association* 2006;**137**:990–8.
2. Rees JS, Addy M. A cross-sectional study of dentine hypersensitivity. *Journal of Clinical Periodontology* 2002;**29**:997–1003.
3. Irwin CR, McCusker P. Prevalence of dentine hypersensitivity in a general dental population. *Journal of the Irish Dental Association* 1997;**43**:7–9.
4. Brannstrom M. The hydrodynamic theory of dentinal pain: sensation in preparations, caries, and the dentinal crack syndrome. *Journal of Endodontics* 1986;**12**:453–7.
5. Brannstrom M, Linden LA, Johnson G. Movement of dentinal and pulpal fluid caused by clinical procedures. *Journal of Dental Research* 1968;**47**:679–82.
6. Ren YF, Amin A, Malmstrom H. Effects of tooth whitening and orange juice on surface properties of dental enamel. *Journal of Dentistry* 2009;**37**:424–31.
7. Ranjitkar S, Rodriguez JM, Kaidonis JA, Richards LC, Townsend GC, Bartlett DW. The effect of casein phosphopeptide-amorphous calcium phosphate on erosive enamel and dentine wear by toothbrush abrasion. *Journal of Dentistry* 2009;**37**:250–4.
8. Prati C, Montebugnoli L, Suppa P, Valdre G, Mongiorgi R. Permeability and morphology of dentin after erosion induced by acidic drinks. *Journal of Periodontology* 2003;**74**:428–36.
9. Murrell S, Marshall TA, Moynihan PJ, Qian F, Wefel JS. Comparison of in vitro erosion potentials between beverages available in the United Kingdom and the United States. *Journal of Dentistry* 2010;**38**:284–9.
10. Brunton PA, Kalsi KS, Watts DC, Wilson NH. Resistance of two dentin-bonding agents and a dentin densensitizer to acid erosion in vitro. *Dental Materials* 2000;**16**:351–5.
11. West N, Addy M, Hughes J. Dentine hypersensitivity: the effects of brushing desensitizing toothpastes, their solid and liquid phases, and detergents on dentine and acrylic: studies in vitro. *Journal of Oral Rehabilitation* 1998;**25**:885–95.
12. Macdonald E, North A, Maggio B, Sufi F, Mason S, Moore C, *et al.* Clinical study investigating abrasive effects of three toothpastes and water in an in situ model. *Journal of Dentistry* 2010;**38**:509–16.
13. Pashley DH, Tay FR, Haywood VB, Collins MA, Drisko CL. Consensus-based recommendations for the diagnosis and management of dentin hypersensitivity. *Compendium of Continuing Education in Dentistry* 2008;**29**:1–36.
14. Wang Z, Sa Y, Sauro S, Chen H, Xing W, Ma X, *et al.* Effect of desensitising toothpastes on dentinal tubule occlusion: a dentine permeability measurement and SEM in vitro study. *Journal of Dentistry* 2010;**38**:400–10.
15. Markowitz K, Pashley DH. Discovering new treatments for sensitive teeth: the long path from biology to therapy. *Journal of Oral Rehabilitation* 2008;**35**:300–15.
16. Hench LL. Bioceramics – from concept to clinic. *Journal of the American Ceramic Society* 1991;**74**:1487–510.
17. Hulbert SF, Bokros JC, Hench LL, Wilson J, Heimke G. Ceramics in clinical applications: past, present and future. Amsterdam, Netherlands: Elsevier; 1987.
18. Yamamuro T, Hench LL, Wilson J. Handbook of bioactive ceramics, vol. II: Calcium phosphate and hydroxyl apatite ceramics. Boca Raton, Florida: CRS Press; 1990.
19. Bakry AS, Takahashi H, Otsuki M, Yamashita K, Tagami J. CO_2 laser improves 45S5 bioglass interaction with dentin. *Journal of Dental Research* 2011;**90**:246–50.
20. Bakry AS, Matin K, Tanaka Y, Otsuki M, Takahashi H, Yamashita K, et al. Evaluating the durability of phosphoric acid promoted bioglass–dentin interaction layer. IADR General Session, Miami, FL; 2009.
21. Kasugai S, Adachi M, Ogura H. Establishment and characterization of a clonal cell line (RPC-C2A) from dental pulp of the rat incisor. *Archives of Oral Biology* 1988;**33**: 887–891.
22. Lan WH, Lan WC, Wang TM, Lee YL, Tseng WY, Lin CP, *et al.* Cytotoxicity of conventional and modified glass ionomer cements. *Operative Dentistry* 2003;**28**:251–9.
23. Charlton DG, Moore BK, Swartz ML. Direct surface pH determinations of setting cements. *Operative Dentistry* 1991;**16**:231–8.
24. Czarnecka B, Limanowska-Shaw H, Hatton R, Nicholson JW. Ion release by endodontic grade glass-ionomer cement. *Journal of Materials Science Materials in Medicine* 2007;**18**: 649–652.
25. Bandyopadhyay-Ghosh S, Reaney IM, Brook IM, Hurrell-Gillingham K, Johnson A, Hatton PV. In vitro biocompatibility of fluorcanasite glass–ceramics for bone tissue repair. *Journal of Biomedical Materials Research A* 2007;**80**:175–83.
26. Munukka E, Lepparanta O, Korkeamaki M, Vaahtio M, Peltola T, Zhang D, *et al.* Bactericidal effects of bioactive glasses on clinically important aerobic bacteria. *Journal of Materials Science Materials in Medicine* 2008;**19**:27–32.
27. Hu S, Chang J, Liu M, Ning C. Study on antibacterial effect of 45S5 bioglass. *Journal of Materials Science Materials in Medicine* 2009;**20**:281–6.
28. Sengun A, Buyukbas S, Hakki SS. Cytotoxic effects of dental desensitizers on human gingival fibroblasts. *Journal of Biomedical Materials Research B Applied Biomaterials* 2006;**78**:131–7.
29. Kolker JL, Vargas MA, Armstrong SR, Dawson DV. Effect of desensitizing agents on dentin permeability and dentin tubule occlusion. *Journal of Adhesive Dentistry* 2002;**4**: 211–221.
30. Bunker BC, Tallant DR, Headley TJ, Turner GL, Kirkpatrick RJ. The structure of leached sodium borosilicate glass. *Journal of Physical Chemistry* 1988;**29**:106–20.
31. Hurrell-Gillingham K, Reaney IM, Brook I, Hatton PV. In vitro biocompatibility of a novel Fe_2O_3 based glass ionomer cement. *Journal of Dentistry* 2006;**34**:533–8.
32. Lim H. Cytotoxicity evaluation of calcium sulfate based temporary filling materials. International Association for Dental Research General Session, San Diego, CA; 2002.
33. Craig RG, Powers JM. Biocompatibility of dental materials. *Restorative dental materials*. 11th ed. St. Louis: Mosby, Inc.; 2002. p. 135.
34. Ter Wee PM, Beelen RH, van den Born J. The application of animal models to study the biocompatibility of bicarbonate-buffered peritoneal dialysis solutions. *Kidney International Supplement* 2003;**88**:75–83.
35. Chen RS, Liu CC, Tseng WY, Jeng JH, Lin CP. Cytotoxicity of three dentin bonding agents on human dental pulp cells. *Journal of Dentistry* 2003;**31**:223–9.
36. Wang JD, Hume WR. Diffusion of hydrogen ion and hydroxyl ion from various sources through dentine. *International Endodontic Journal* 1988;**21**:17–26.

Society For Biomaterials

Evaluation of the osteoconductivity of α-tricalcium phosphate, β-tricalcium phosphate, and hydroxyapatite combined with or without simvastatin in rat calvarial defect

Hisham Rojbani,[1] Myat Nyan,[1] Keiichi Ohya,[2] Shohei Kasugai[1]

[1]Oral Implantology and Regenerative Dental Medicine, Graduate School, Tokyo Medical and Dental University, 1-5-45 Yushima, Bunkyo, Tokyo 113-8549, Japan
[2]Pharmacology, Department of Hard Tissue Engineering, Graduate School, Tokyo Medical and Dental University, Tokyo 113-8549, Japan

Received 7 September 2010; revised 8 January 2011; accepted 17 March 2011
Published online 16 June 2011 in Wiley Online Library (wileyonlinelibrary.com). DOI: 10.1002/jbm.a.33117

Abstract: The purpose of this study is to evaluate the osteoconductivity of three different bone substitute materials: α-tricalcium phosphate (α-TCP), (β-TCP), and hydroxyapatite (HA), combined with or without simvastatin, which is a cholesterol synthesis inhibitor stimulating BMP-2 expression in osteoblasts. We used 72 Wistar rats and prepared two calvarial bone defects of 5 mm diameter in each rat. Defects were filled with the particles of 500–750 μm diameter combined with or without simvastatin at 0.1 mg dose for each defect. In the control group, defects were left empty. Animals were divided into seven groups: α-TCP, β-TCP, HA, α-TCP with simvastatin, β-TCP with simvastatin, HA with simvastatin, and control. The animals were sacrificed at 6 and 8 weeks. The calvariae were dissected out and analyzed with micro CT. The specimens were evaluated histologically and histomorphometrically. In α-TCP group, the amount of newly formed bone was significantly more than both HA and control groups but not significantly yet more than β-TCP group. Degradation of α-TCP was prominent and β-TCP showed slower rate while HA showed the least degradation. Combining the materials with Simvastatin led to increasing in the amount of newly formed bone. These results confirmed that α-TCP, β-TCP, and HA are osteoconductive materials acting as space maintainer for bone formation and that combining these materials with simvastatin stimulates bone regeneration and it also affects degradability of α-TCP and β-TCP. Conclusively, α-TCP has the advantage of higher rate of degradation allowing the more bone formation and combining α-TCP with simvastatin enhances this property. © 2011 Wiley Periodicals, Inc. J Biomed Mater Res Part A: 98A: 488–498, 2011.

Key Words: osteoconductivity, α-tricalcium phosphate, simvastatin, degradation.

How to cite this article: Rojbani H, Nyan M, Ohya K, Kasugai S. 2011. Evaluation of the osteoconductivity of α-tricalcium phosphate, β-tricalcium phosphate, and hydroxyapatite combined with or without simvastatin in rat calvarial defect. J Biomed Mater Res Part A 2011:98A:488–498.

INTRODUCTION

The number of clinicians performing endosseous dental implants whether immediately following tooth extraction or after a period of time is rapidly increasing. However, on many occasions clinicians encounter the lack of adequate amount of bone due to a number of reasons including injury, eradicated tumor masses, or progressive periodontal diseases. To overcome this difficulty, many methods have been developed and introduced using a variety of grafts such as autologous bone grafts, allografts, alloplasts, and xenografts.[1] Autologous bone is regarded as one of the gold standard of graft materials.[2–4] However, there are several problems in autologous bone grafts including morbidity of the donor site and limitation of amount of bone that can be harvested.[5,6] It is becoming a demand to identify different types of bone substitutes. Moreover, the process of osteogenesis can be stimulated by applying bone formation stimulating molecules.[7–9] Calcium phosphates, such as tricalcium phosphate (TCP), and hydroxyapatite (HA) are widely used as substitutes for autologous bone.[10,11] These materials show high biocompatibility and osteoconductivity.[12] HA is a biomaterial with a lower degradation rate than new bone formation *in vivo*.[13,14] On the other hand, the degradation rate of TCP is higher than HA *in vivo*. α-TCP dissolves more easily in water than β-TCP even though they have exactly the same chemical composition. However, it is important for a bone substitute material to have the character of degradation rate equal to the process of bone formation.

Interestingly, simvastatin, an inhibitor of cholesterol synthesis, stimulates BMP-2 expression in osteoblasts.[15] We have recently reported that α-TCP containing simvastatin stimulates bone regeneration in rat calvarial defects by enhancing BMP-2 expression.[16] The purpose of this study was to evaluate osteoconductivity of three different calcium phosphate materials, α-TCP, β-TCP, and HA, combined with or without simvastatin in rat calvarial defects.

Correspondence to: H. Rojbani; e-mail: hisham.rojbani@gmail.com

TABLE I. List of the Experimental Groups

Group	Bone Substitute	Simvastatin	Number of Defects
1	α-TCP	−	12
2	α-TCP	+	12
3	β-TCP	−	12
4	β-TCP	+	12
5	HA	−	12
6	HA	+	12
7	Control	−	12

MATERIALS AND METHODS

This study was approved by the institutional committee of animal experiments. Bone substitute particles of α-TCP, β-TCP, and HA of 500–750 μm diameter were kindly supplied by (Advance, Co., Tokyo, Japan). Simvastatin powder (Merck & Co., Whitehouse Station, NJ) was dissolved in ethanol (Wako Pure Chemical Industries, Osaka) and incorporated into each bone substitute particles. The amount of simvastatin in 1 mg bone substitute particles was 7 μg and each calvarial defect received approximately 14 mg bone substitute particles. Thus, finally 0.1 mg simvastatin was applied in each calvarial defect.

Seventy two male Wistar rats (14-week old about 250–350 g) were divided into seven groups, α-tricalcium phosphate (α-TCP), β-tricalcium phosphate (β-TCP), hydroxyapatite (HA), α-TCP with simvastatin, β-TCP with simvastatin, HA with simvastatin, and the control (Table I).

Surgical procedures

The animals were anesthetized with a combination of ketamine (40 mg/kg)–xylazine (5 mg/kg), In addition, 0.2 mL of local anesthetic (2% xylocaine/epinephrine 1:20,000, Fujisawa, Tokyo, Japan) was injected into the surgical sites before the start of surgery. The surgical areas were shaved and disinfected with povidone-iodine (Isodine Surgical Scrub, Meiji, Tokyo, Japan), skin incision, and subperiosteal dissection were carried out, a flap was raised and bone defect of 5 mm diameter was prepared reaching the dura mater of the brain on each side lateral to the sagittal plane with a bone trephine bur. The defects were filled with bone substitute particles according to the group. The control group defects were left unfilled. The periosteoum was repositioned and sutured with a 4-0 Vicryl polyglactin suture (Ethicon, NJ) and the skin was sutured by 4-0 silk (ELP Akiyima Co., Tokyo, Japan) (Fig. 1). The animals were injected subcutaneously for the bone labeling with calcein and tetracycline 7 days and 1 day, respectively, before sacrifice for the histomorphometric analysis. The animals were sacrificed at 6 and 8 weeks after the surgery.

Micro CT and computer analysis

After sacrificing the animals, the calvaria were dissected out and fixed in neutral 10% formalin then examined with soft X-ray radiography and dual-energy X-ray absorptiometry for small animals (DCS-600; Aloka Co., Tokyo). Furthermore micro CT (InspeXio; Shimadzu Science East Corporation, Tokyo) was conducted. Micro CT images were analyzed with Tri/3D-Bone software (RATOC System Engineering Co., Tokyo, Japan). Bone volume (BV), bone mineral contents (BMC), bone mineral density (BMD), and remaining bone substitute particles were measured within the region of interest (ROI).

Histological processing

Specimens were prepared for either paraffin wax embedding for the decalcified sectioning or methyl methacrylate (MMA) embedding for the undecalcified sectioning. Decalcification was carried out by immersing the specimens in 10% EDTA for 4 weeks. Decalcified specimens were dehydrated in ascending

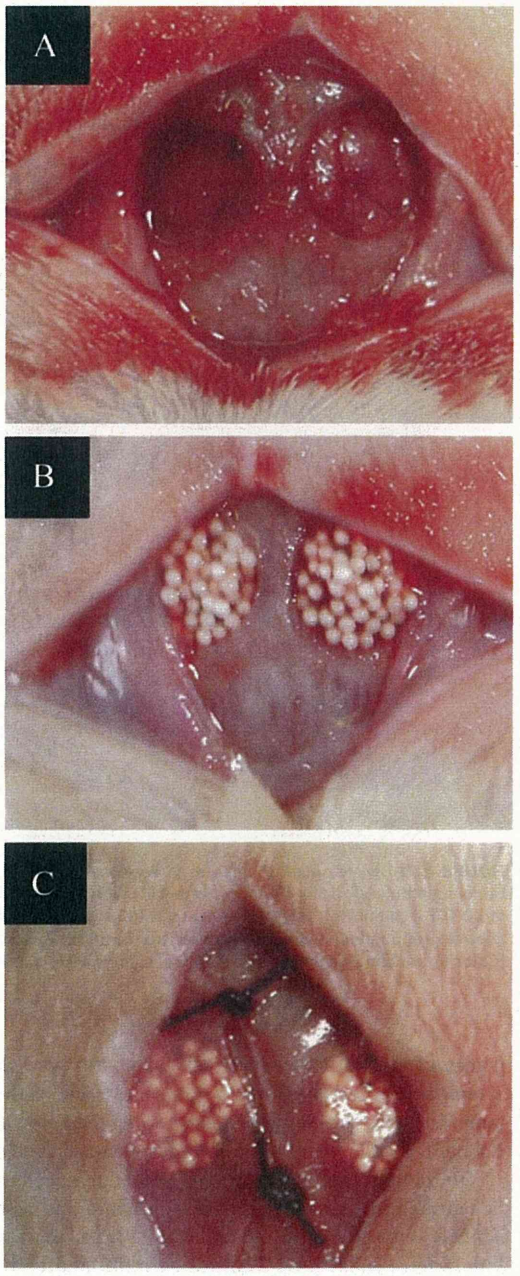

FIGURE 1. Photos of surgical procedures. Subperiosteal dissection (A), bone substitute material applied to the 5 mm defects in the calvarial bone (B), and suturing periosteum with resorbable suture (C).

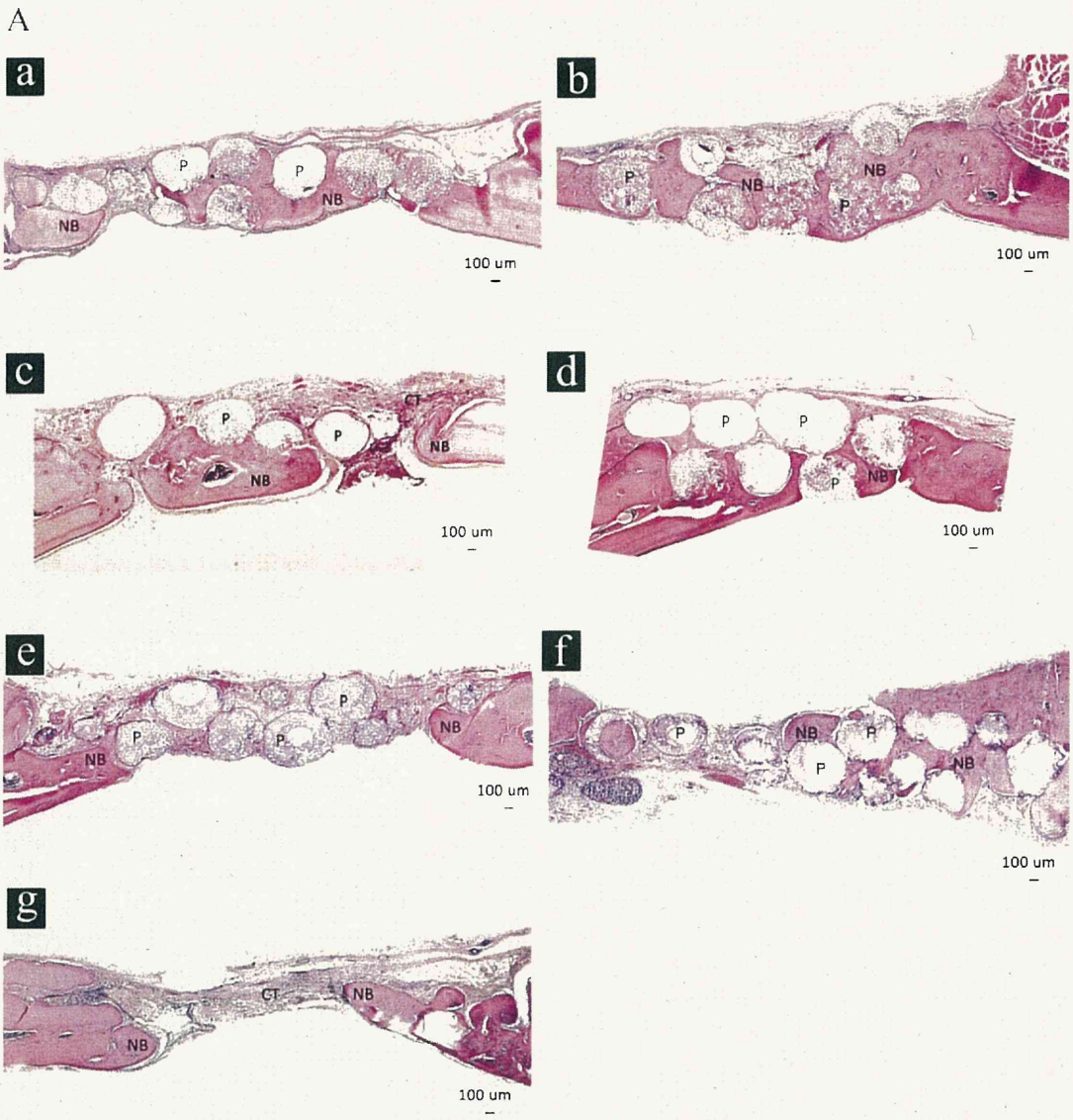

FIGURE 2. (A) Histological images at 6 weeks, α-TCP (a), α-TCP+statin (b), β-TCP (c), β-TCP+statin (d), HA (e), HA+statin (f), and Control (g). Bone substitute particles (P), new bone (NB), and connective tissue (CT). (B) Histological images at 8 weeks. α-TCP (a), α-TCP + statin (b), β-TCP (c), β-TCP + statin (d), HA (e), HA + statin (f), and control (g). Bone substitute particles (P), new bone (NB), and connective tissue (CT). Bone in control group failed to progress toward the center of the defect (g). α-TCP particles were progressively degraded and replaced by new bone (b). [Color figure can be viewed in the online issue, which is available at wileyonlinelibrary.com.]

grades of ethanol and embedded in paraffin wax. Embedded samples were sectioned into 7 μm serial slices with a microtome, following the coronal direction along the defect and calvarial bone. Sections were stained with hematoxylin and eosin.

To obtain undecalcified sections, the specimens were dehydrated in ascending grades of ethanol and acetone and stained with Villanueva bone stain (Wako Pure Chemical Industries, Osaka) for 15 days then infiltrated with and embedded in MMA resin. The MMA embedded sections were cut with a microtome to a thickness about 50 μm following the coronal direction along the defect and calvarial bone.

Histomorphometrical analysis

Both calcified and undecalcified specimens were examined under light microscope (Biozero, BZ-8000; Keyence, Osaka, Japan) for the evaluation of new bone formation among the groups. Fluorescent microscope was used to evaluate the mineral apposition rate (MAR) in the undecalcified samples within one week. Imaging software (ImageJ 1.42q, Wayne Rasband, National Institute of Health) was used to measure the percentage of new bone formation, percentage of remaining bone substitute materials, and MAR.

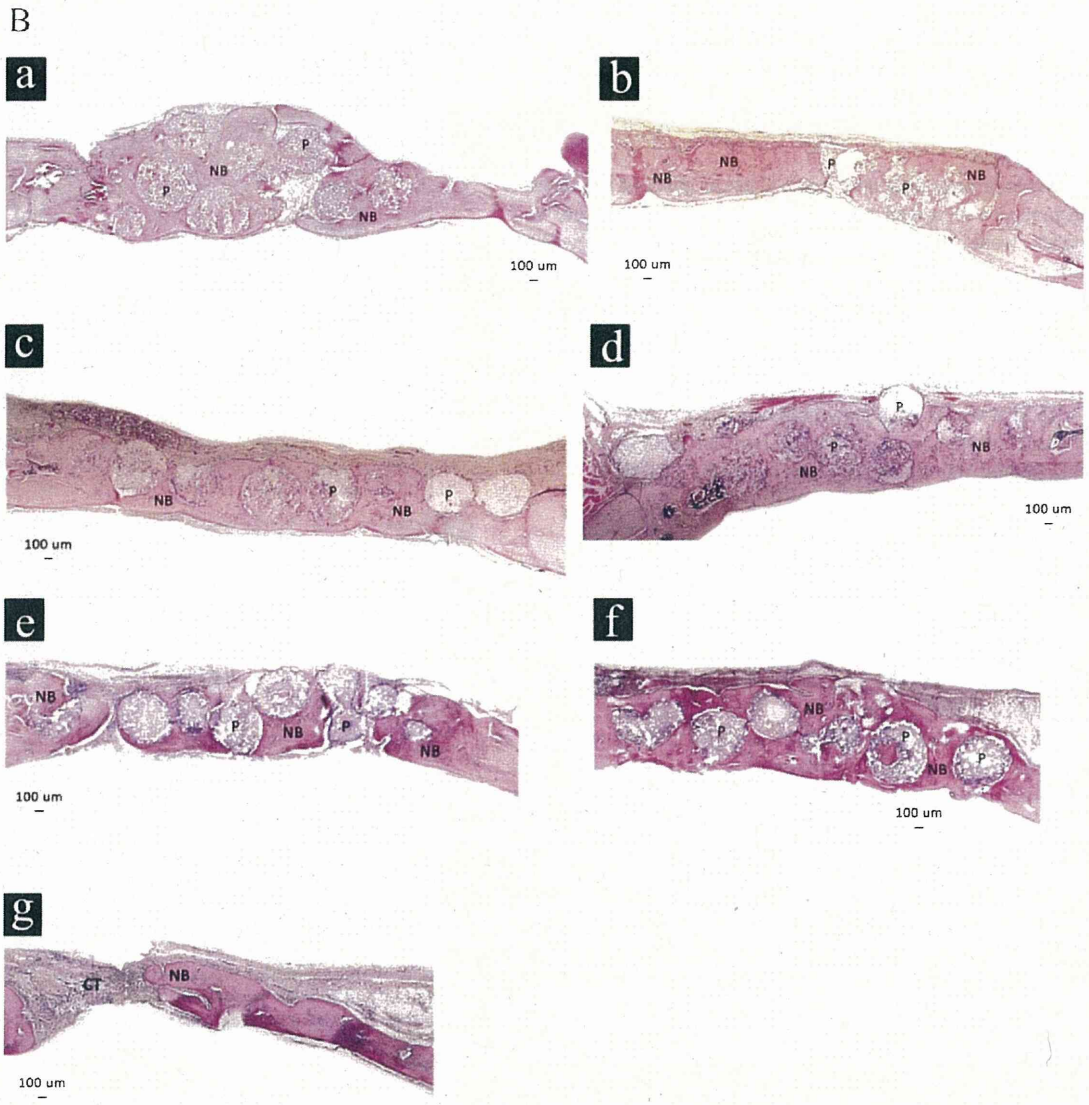

FIGURE 2. Continued

Statistical analysis

For the numerical data gathered, statistical analysis was performed by commercial software (SPSS) with One-way analysis of variance (ANOVA), where results suggested a significant difference between groups ($p < 0.05$). The data were further analyzed by *Tukey's post hoc* multiple comparisons test.

RESULTS

Macroscopic observation

During the recovery phase, no macroscopic infection of the wound was noted. However, all simvastatin groups showed a reddish inflammation in the skin area overlying the bone defects, the inflammation was subsided to a normal skin within 10 days. The wounds showed a complete healing after 2 weeks.

Histological observation

The histological images are presented in Figures 2–4.

Control groups

In both 6 and 8 weeks, the new bone failed to progress toward the center of the defect and only a thin layer of new bone was seen at the defect margins. The central portion of defect was filled with compressed fibrous connective tissue [Fig. 2(A-g,B-g)].

α-TCP groups

In 6 weeks group, the defects were filled with new bone islands between the particles with the presence of woven bone. The particles are starting to degrade and partially replaced by new bone [Fig. 2(A-a)]. In 8 weeks group, more bone was taking place of the degraded particles, and there was more bone formation in between the particles [Fig. 2(B-a)].

In 6 weeks with simvastatin group, the defects were not completely filed with bone, the particles were ongoing

degradation and replaced mostly by woven bone [Fig. 2(A-b)]. In 8 weeks with simvastatin group, the new bone filled the defect almost completely, and the particles are also mostly replaced by new bone [Fig. 2(B-b)].

β-TCP groups

In 6 weeks group, new bone took place in parts of the defect with presence of woven bone and some connective tissue, the particles were slightly degraded [Fig. 2(A-c)]. In 8 weeks group, the new bone was occupying most of the defects, and the particles were further degraded [Fig. 2(B-c)].

In 6 weeks with simvastatin group, the new bone took place in more parts of the defect in comparison with the non simvastatin group, and the particles are also slightly degraded [Fig. 2(A-d)]. In 8 weeks with simvastatin group, the new bone was filling the defects almost completely, and the particles were further degraded and replaced by new bone [Fig. 2(B-d)].

HA groups

In 6 weeks, the new bone took place at the margins of the defects, woven bone was filling the center of the defects and spaces between particles, the particles showed no degradation [Fig. 2(A-e)]. In 8 weeks, the new bone was filling the spaces between particles, and the particles showed least degradation [Fig. 2(B-e)].

In 6 weeks simvastatin group, parts of the defects were filled with new bone while other parts were filled with woven bone, and the particles showed no degradation [Fig. 2(B-f)]. In 8 weeks with simvastatin group, more bone was filling the defects in comparison with the non simvastatin group, and particle also showed least degradation [Fig. 2(B-f)].

As shown in Figure 3, the group of HA with simvastatin showed significant increase in number of osteoblastic cells compared with the group without simvastatin, which was also evident in the groups of α-TCP and β-TCP with/without simvastatin. The pattern of bone formation suggests that the osteoblastic cells were differentiated from the dura mater.

Degradation of the materials

There was a significant difference in the degradability of the three bone substitute materials. As for the α-TCP particles almost all the particles had degraded after 8 weeks, while β-TCP showed degradation to some extent but significantly less than α-TCP. HA particles showed least amount of degradation and can be clearly observed (Fig. 4).

Radiological findings

Control groups. In both 6 and 8 weeks showed scanty amount of thin bone extending toward the center but failed to fill the defect [Fig. 5(A-g,B-g)].

α-TCP groups. In 6 and 8 weeks particles were reduced in size, less radio opaque and well integrated with significant amount of new bone [Fig. 5(A-a,B-a)]. Simvastatin groups were showing more amount of new bone and the opacity of the particles is almost similar to the bone which can be clearly observed in α-TCP + statin 8 weeks group [Fig. 5(A-b,B-b)].

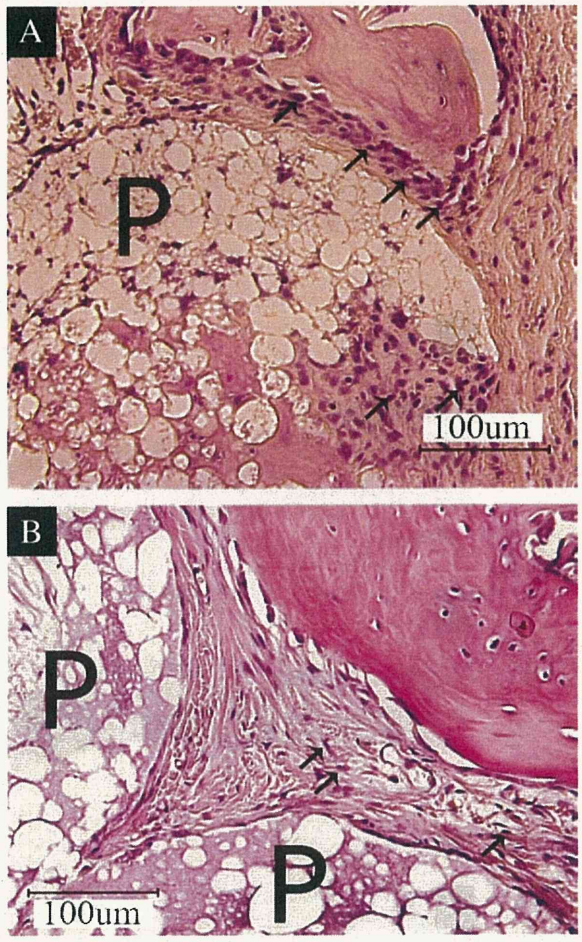

FIGURE 3. Higher magnified histological images of HA group with simvastatin (A) and without simvastatin (B) at 6 weeks. Bone substitute particles (P) and osteoblastic cells (arrows). [Color figure can be viewed in the online issue, which is available at wileyonlinelibrary.com.]

β-TCP groups. At 6 weeks, newly formed bone and β-TCP particles could be easily differentiated as they revealed different radiopacity [Fig. 5(A-c)], in simvastatin group more bone is observed [Fig. 5(A-d)]. At 8 weeks, particles are slightly reduced in size and more new bone can be observed, in simvastatin group no difference in particles size can be seen but more new bone is formed [Fig. 5(B-c,B-d)].

HA groups. At 6 and 8 weeks particles showed least reduction in size for both non simvastatin and simvastatin groups [Fig. 5(A-e,f,B-e,f)]. Bone formation was scattered between the particles in 6 weeks group [Fig. 5(A-e)], but it appears to fill in between particles in statin group [Fig. 5(A-f)]. In 8 weeks, statin group showed higher amount of new bone than non- statin group [Fig. 5(B-e,f)].

DISCUSSION

Although autologous graft is the golden standard for the graft materials,[17,18] it is not always possible to harvest sufficient amount of bone due to factors such as the limitation

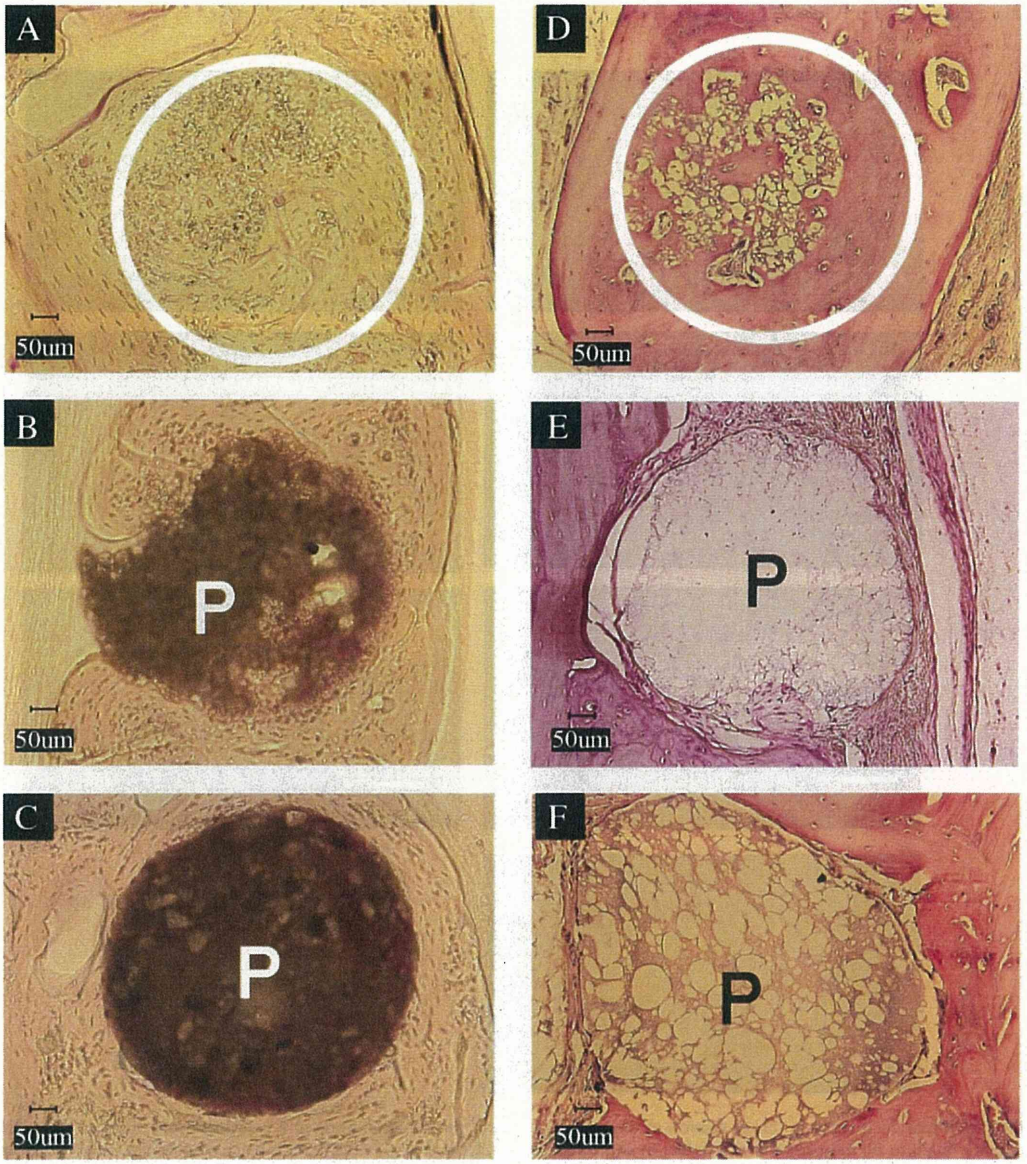

FIGURE 4. Histological images representing degradability between the three types of bone substitutes at 8 weeks. α-TCP particles are the most degraded (A,D), followed by β-TCP (B,E), while HA particles are the least degraded and can be clearly seen (C,F). Circles in (A,D) indicates the area of the degraded particles. α-TCP (A), β-TCP (B), HA (C) (Villanueva bone stain), α-TCP (D), β-TCP (E), HA (F) (H&E stain). [Color figure can be viewed in the online issue, which is available at wileyonlinelibrary.com.]

of donor sites.[19–21] Therefore many researchers have investigated calcium phosphate as bone graft material because of its good biocompatibility,[12,22] it was introduced successfully as a bone substitute material. Although bone substitutes currently available are osteoconductive, more effective material is clinically desired. In this study, the osteoconductivity of three different bone substitute materials was evaluated in bilateral rat calvarial model. In Figure 6(A,B) the quantitative results show the percentage of new bone formation among 6 and 8 weeks groups. In α-TCP + statin group, the percentage was the highest compared with the other bone substitute materials, while in control group the percentage was the lowest. Furthermore, the percentage was significantly higher within the same material when simvastatin was added in both α-TCP and β-TCP groups, while no significance was found in the HA group, however the percentage has a tendency to increase when simvastatin was added to HA particles. Accordingly, the results of this study suggest that TCP was better osteoconductive than HA and this can be attributed to the biodegradability of the TCP which led into significance in the results. Despite the degradability of α-TCP over β-TCP, there was no significant difference in the percentage of new bone formed among these two TCP materials [Fig. 6(A,B)]. The rate of bone formation versus particle

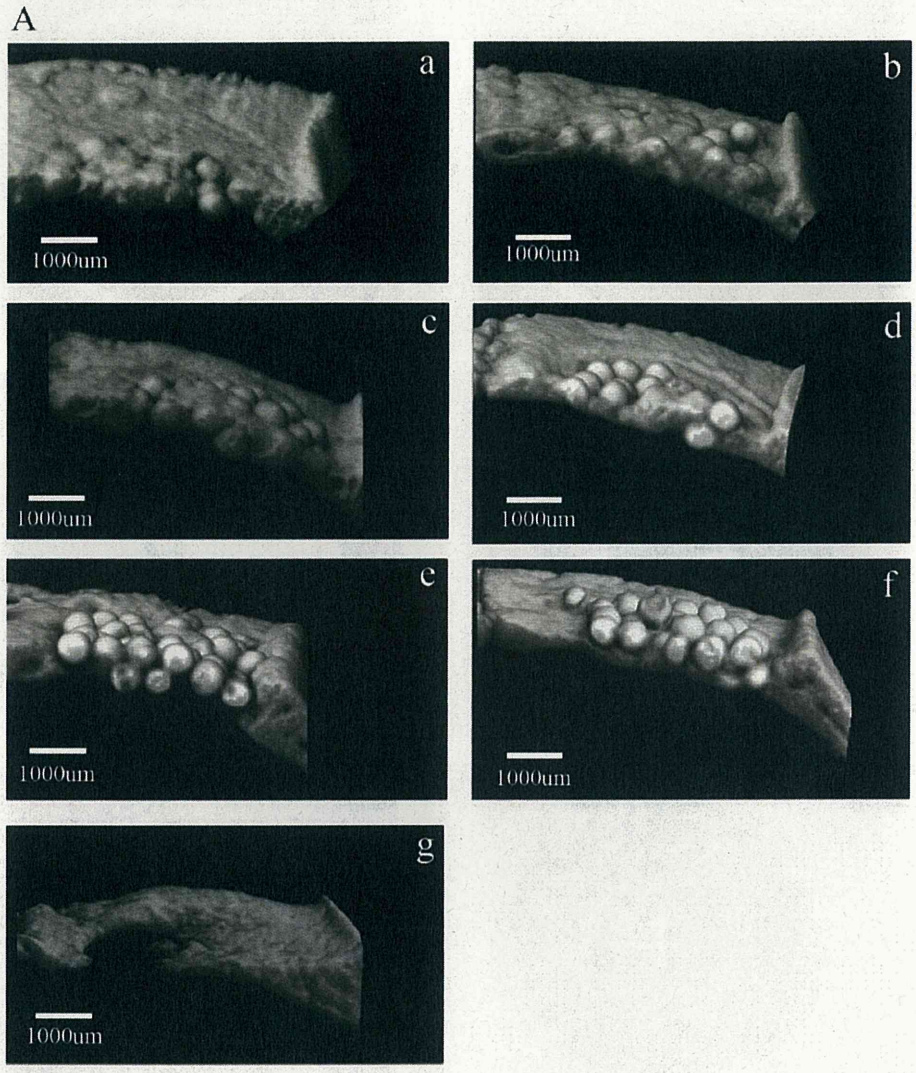

FIGURE 5. (A) Micro CT images for cross section in the coronal plane of the calvarial bone at 6 weeks, slightly tilted to show the region of interest. The bone failed to fill the center of the defect in control group (g). Note that α-TCP (Alpha tricalcium phosphate) particles are less radio opaque (a,b) when compared with the other two types. α-TCP (a), α-TCP + statin (b), β-TCP (c), β-TCP + statin (d), HA (e), HA + statin (f), and Control (g). (B) Micro CT images for cross section in the coronal plane of the calvarial bone at 8 weeks, slightly tilted to show the region of interest. α-TCP (a), α-TCP + statin (b), β-TCP (c), β-TCP + statin (d), HA (e), HA + statin (f), and Control (g).

degradation is an important factor. Therefore, the ideal bone substitute material can be defined as the one that degrades in synchronous manner with the bone formation. It has been reported that the ideal graft substitute should reabsorb with time to allow and encourage new bone formation whilst maintaining its properties as an osteoconductive scaffold until it is no longer required.[23] In this study, quantitative results of the remaining bone substitute materials demonstrated that after 6 and 8 weeks, less than 10% of α-TCP particles remained [Fig. 7(A,B)]. Consequently, this study suggests that α-TCP is the material of choice among the tested substitutes due to the higher degradability rate which may provide sufficient space for bone formation. However, based on histological observation and quantitative analysis it was noticed that the degradation rate of α-TCP is slightly higher than the bone formation rate [Fig. 4(A,D)], but it was within the acceptable rate, as α-TCP successfully acted as a space maintainer, scaffold, and osteoconductive material.

Simvastatin is an inhibitor of cholesterol synthesis that has the effect of stimulating bone formation.[16,24,25] Previous studies showed that it stimulates the BMP-2 expression in osteoblasts and that it also inhibits the osteoclastic activity.[26–29] Thus, it is reasonable to expect that combining a bone substitute with simvastatin favorably modifies the material character by stimulating bone formation. In this study, the highest BMC and BMD in 6 and 8 weeks were found when combining simvastatin with α-TCP (Tables II and III). The simvastatin dose in this study was determined

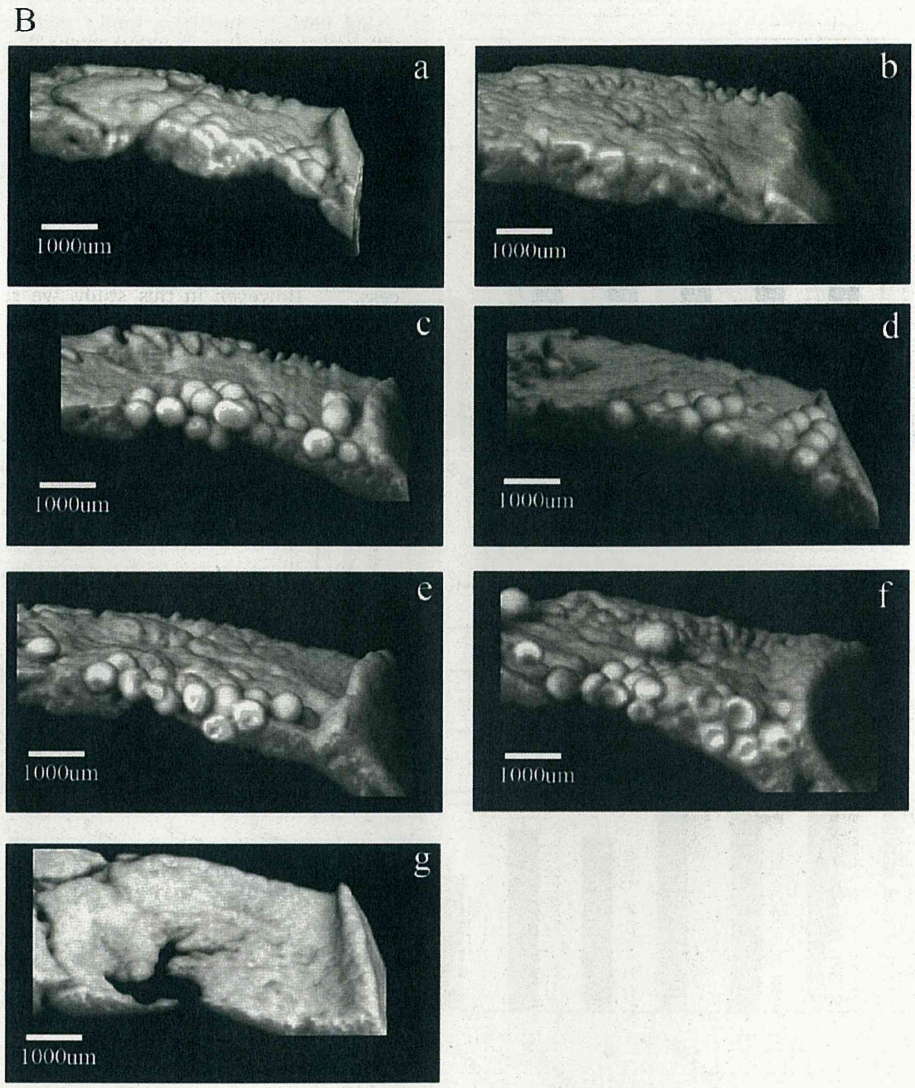

FIGURE 5. Continued

according to our previous study that showed that optimum dose for the same defect sizes was 0.1 mg. In the previous study, a higher dose led to inflammation of the skin above the defects while lower dose did not stimulate bone formation.[30] However, in this study, skin inflammation was observed over the applied area although this inflammation was slight and temporal. The releasing mechanism of the simvastatin from the materials is not clear. The drug release from the material would be affected by the solubility of the drug in the surrounding solution, the binding strength of the drug to the material, the material porosity and the material degradation speed. Our previous *in vitro* study demonstrated that more than half of the simvastatin was released from α-TCP particles on the first day, which was followed by slow release of the drug.[26] The releasing profile of the drug from the three materials *in vivo* is different because the degradation rate of the materials strongly affects the drug release. However, it is likely that the initial burst of drug release from the materials also occurred *in vivo* in this study. It would be much beneficial to control the release of the simvastatin on the basis of a daily dose,[31] this could secure a sustained stimulation of the bone formation for appropriate period of time.

In our previous study, combining α-TCP with simvastatin stimulated MAR compared with the one of α-TCP alone. However, in this study, the MAR was not stimulated when the materials were combined with simvastatin at the same dose (Tables II and III). This is probably due to the difference of the time points of the histomorphometrical measurement: 4 and 6 weeks in the previous study; 6 and 8 weeks in this study due to that the most of the simvastatin has been released at an earlier time. Furthermore, it would be also possible that there were differences in the microstructure and/or crystal size between the previous

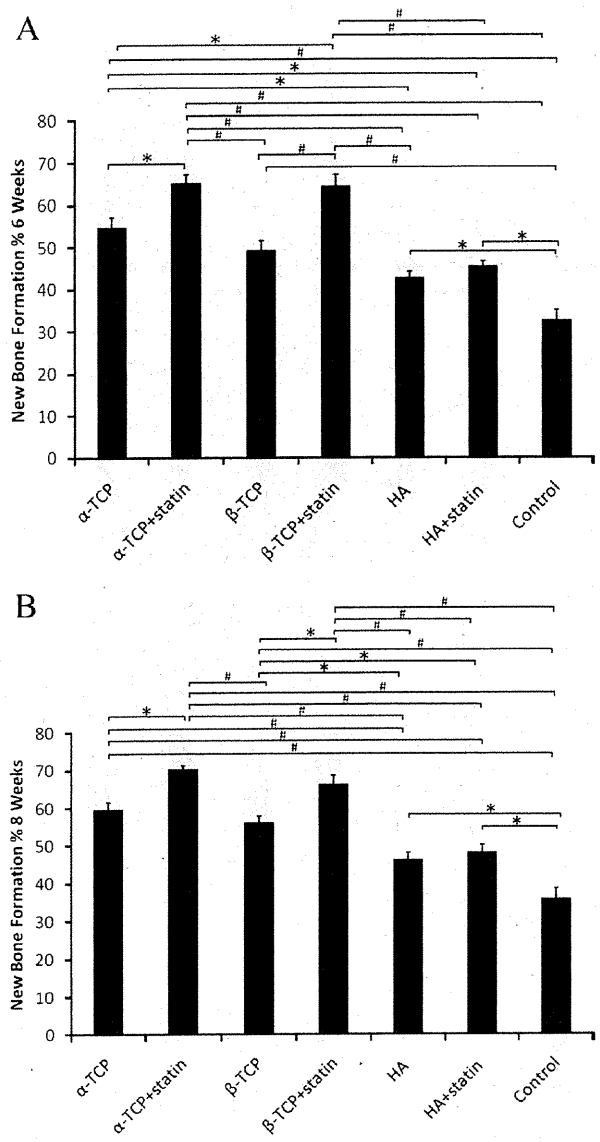

FIGURE 6. (A) Percentage of new bone formation in 6 weeks. $^{*}p \leq 0.05$, $^{\#}p < 0.001$. Values are shown as mean ± SEM. The highest percentage of new bone formation was found in α-TCP with statin group. Statin had a significant role in new bone formation among the two TCP bone substitutes, however, no significance was observed when using statin in HA particles. (B) Percentage of new bone formation in 8 weeks. $^{*}p \leq 0.05$, $^{\#}p < 0.001$. Values are shown as mean ± SEM. The percentage of new bone formation was slightly increased compared with 6 weeks.

and the present materials, which affected the releasing speed of the drug from the materials. The temporal inflammatory response of the skin on the applied area in this study, which was not observed in the previous study, could be probably explained by higher rate of drug release from the materials in this study compared with the previous study.

The pattern of bone formation suggests that the osteoprogenitor cells are differentiated from the dura mater. The number of osteoblast cells was significantly higher in the simvastatin groups compared with non simvastatin groups. This can be attributed to the role of simvastatin in stimulating BMP-2 which is a family member of the Transforming growth factor beta protein (TGF-β) that controls proliferation, and cellular differentiation.[32–35]

The defect size used in this study was 5 mm in diameter, which can be considered critical as new bone formation in most defects failed to fill the center after 8 weeks in the control group. The bone substitute particles size used in this study was about 500–750 μm, the particle size was found to influence the outcome of the bone formation process.[36,37] However, in this study, we standardized the size and the microstructure of the three materials to eliminate the potential effect of these factors on bone formation.

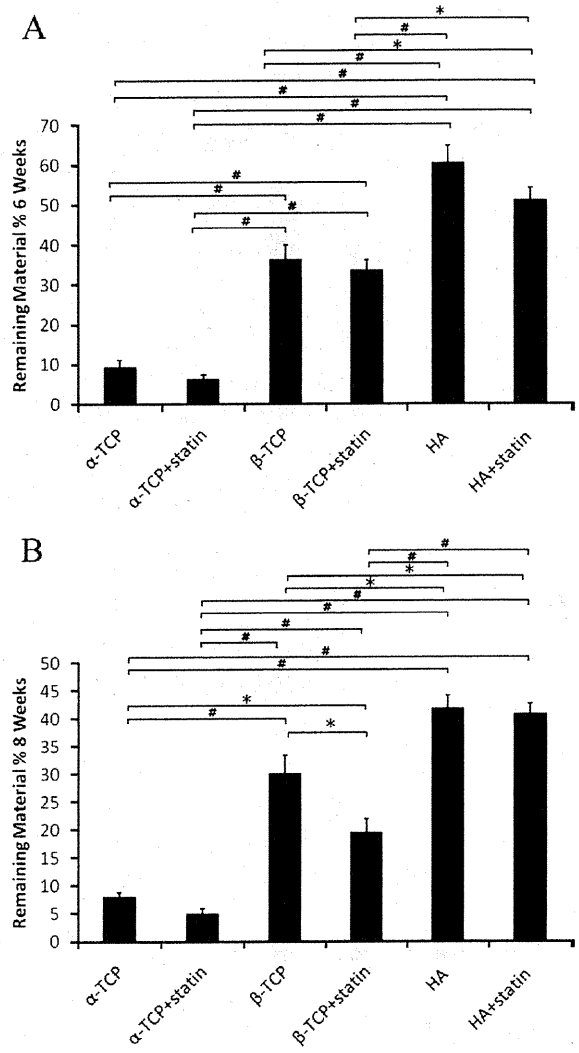

FIGURE 7. (A) Percentage of remaining material in 6 weeks. $^{*}p \leq 0.05$, $^{\#}p < 0.001$. Values are shown as mean ± SEM. The degraded α-TCP particles are significantly higher than the other two bone substitute materials which may potentially create room for more bone formation. (B) Percentage of remaining material in 8 weeks. $^{*}p \leq 0.05$, $^{\#}p < 0.001$. Values are shown as mean ± SEM. Interestingly, the combination of the bone substitute materials with simvastatin affected the degradation of the materials.

TABLE II. Mineral Apposition Rate (MAR), Bone Mineral Contents (BMC), and Bone Mineral Density (BMD) in 6 Weeks

Experimental Group	MAR (μm)	BMC (mg)	BMD (mg/mm^3)
α-TCP	4.32 ± 0.24	13.04 ± 1.05	1.06 ± 0.02
α-TCP+statin	5.20 ± 0.55	13.79 ± 0.79	1.26 ± 0.02
β-TCP	3.14 ± 0.33	10.90 ± 0.46	1.04 ± 0.01
β-TCP+statin	3.44 ± 0.44	12.08 ± 0.42	1.16 ± 0.007
HA	2.67 ± 0.20	10.80 ± 0.39	1.02 ± 0.01
HA+statin	3.1 ± 0.10	11.51 ± 0.45	1.10 ± 0.02
Control	2.16 ± 0.24	8.21 ± 0.04	0.97 ± 0.009

One-way ANOVA with Tukey's post-hoc multiple comparison: $^*p \leq 0.05$, $^\#p < 0.001$. Values are shown as mean ± SEM.

TABLE III. Mineral Apposition Rate (MAR), Bone Mineral Contents (BMC), and Bone Mineral Density (BMD) in 8 Weeks

Experimental Group	MAR (μm)	BMC (mg)	BMD (mg/mm^3)
α-TCP	2.68 ± 0.42	13.13 ± 0.33	1.25 ± 0.01
α-TCP+statin	3.65 ± 0.14	15.26 ± 0.67	1.30 ± 0.02
β-TCP	2.79 ± 0.11	13.33 ± 0.74	1.21 ± 0.01
β-TCP+statin	2.91 ± 0.26	14.45 ± 1.05	1.23 ± 0.01
HA	1.91 ± 0.18	12.53 ± 0.70	1.19 ± 0.008
HA+statin	2.22 ± 0.16	13.36 ± 0.53	1.21 ± 0.016
Control	1.38 ± 0.05	8.91 ± 0.71	1.12 ± 0.009

One-way ANOVA with Tukey's post-hoc multiple comparison: $^*p \leq 0.05$, $^\#p < 0.001$. Values are shown as mean ± SEM.

This study confirmed the difference in the order of degradability of the three materials; α-TCP is the most degradable followed by β-TCP, and HA is the least degradable [Figs. 4 and 7(A,B)]. Interestingly, the combination of the bone substitute materials with simvastatin affected not only bone formation but also the material degradation. Degradation of α-TCP and β-TCP is affected by the solubility of these materials. In addition, it is possible that the degradation of these materials is strongly affected by the bone remodeling speed around the materials, which could explain the more degradation of α-TCP and β-TCP in the simvastatin groups.

CONCLUSION

This study confirmed that α-TCP, β-TCP, and HA are osteoconductive materials acting as space maintainer for bone formation when applied to a bone defect, and demonstrated that combining these materials with simvastatin stimulates bone regeneration and it also affects degradability of α-TCP and β-TCP. Conclusively, α-TCP has the advantage of higher rate of degradation allowing the more bone formation and combining α-TCP with simvastatin enhances this property.

REFERENCES

1. John HD, Wenz B. Histomorphometric analysis of natural bone mineral for maxillary sinus augmentation. Int J Oral Maxillofac Implants 2004;19:199–207.
2. Boyne PJ, James RA. Grafting of the maxillary sinus floor with autogenous marrow and bone. J Oral Surg 1980;38:613–616.
3. Brugnami F, Caiazzo A, Leone C. Local intraoral autologous bone harvesting for dental implant treatment: Alternative sources and criteria of choice. Keio J Med 2009;58:24–28.
4. Moy PK, Lundgren S, Holmes RE. Maxillary sinus augmentation: Histomorphometric analysis of graft materials for maxillary sinus floor augmentation. J Oral Maxillofac Surg 1993;51:857–862.
5. Younger EM, Chapman MW. Morbidity at bone graft donor sites. J Orthop Trauma 1989;3:192–195.
6. Yuan H, Yang Z, De Bruij JD, De Groot K, Zhang X. Material-dependent bone induction by calcium phosphate ceramics: A 2.5-year study in dog. Biomaterials 2001;22:2617–2623.
7. Kasugai S. Local application of statin for bone augmentation. Clin Calcium 2005;15:67–72.
8. Kasugai S, Fujisawa R, Waki Y, Miyamoto K, Ohya K. Selective drug delivery system to bone: Small peptide (Asp)6 conjugation. J Bone Miner Res 2000;15:936–43.
9. Li F, Zhao X, Wu J. Repair of bone defect with allograft demineralized bone containing basic fibroblast growth factor in rabbits. Zhongguo Xiu Fu Chong Jian Wai Ke Za Zhi 2005;19:431–434.
10. Santos FA, Pochapski MT, Martins MC, Zenobio EG, Spolidoro LC, Marcantonio E. Comparison of biomaterial implants in the dental socket: Histological analysis in dogs. Clin Implant Dent Relat Res 2010;12:18–25.
11. Smeets R, Grosjean MB, Jelitte G, Heiland M, Kasaj A, Riediger D, Yildirim M, Spiekermann H, Maciejewski O. Hydroxyapatite bone substitute (Ostim) in sinus floor elevation. Maxillary sinus floor augmentation: Bone regeneration by means of a nanocrystalline in-phase hydroxyapatite (Ostim). Schweiz Monatsschr Zahnmed 2008;118:203–212.
12. Alcaide M, Serrano MC, Pagani R, Sanchez-Salcedo S, Vallet-Regi M, Portoles MT. Biocompatibility markers for the study of interactions between osteoblasts and composite biomaterials. Biomaterials 2009;30:45–51.
13. Kihara H, Shiota M, Yamashita Y, Kasugai S. Biodegradation process of alpha-TCP particles and new bone formation in a rabbit cranial defect model. J Biomed Mater Res B Appl Biomater 2006;79:284–291.
14. Yamaguchi K, Hirano T, Yoshida G, Iwasaki K. Degradation-resistant character of synthetic hydroxyapatite blocks filled in bone defects. Biomaterials 1995;16:983–985.
15. Mundy G, Garrett R, Harris S, Chan J, Chen D, Rossini G, Boyce B, Zhao M, Gutierrez G. Stimulation of bone formation in vitro and in rodents by statins. Science 1999;286:1946–1949.
16. Nyan M, Sato D, Oda M, Machida T, Kobayashi H, Nakamura T, Kasugai S. Bone formation with the combination of simvastatin and calcium sulfate in critical-sized rat calvarial defect. J Pharmacol Sci 2007;104:384–386.
17. Giannoudis PV, Dinopoulos H, Tsiridis E. Bone substitutes: An update. Injury 2005;36(Suppl 3):S20–S27.
18. Rueger JM. Bone substitution materials. Current status and prospects. Orthopade 1998;27:72–79.
19. Baqain ZH, Anabtawi M, Karaky AA, Malkawi Z. Morbidity from anterior iliac crest bone harvesting for secondary alveolar bone grafting: An outcome assessment study. J Oral Maxillofac Surg 2009;67:570–575.
20. Beirne JC, Barry HJ, Brady FA, Morris VB. Donor site morbidity of the anterior iliac crest following cancellous bone harvest. Int J Oral Maxillofac Surg 1996;25:268–271.
21. Swan MC, Goodacre TEE. Morbidity at the iliac crest donor site following bone grafting of the cleft alveolus. Br J Oral Maxillofac Surg 2006;44:129–133.
22. Yoshimine Y, Akamine A, Mukai M, Maeda K, Matsukura M, Kimura Y, Makishima T. Biocompatibility of tetracalcium phosphate cement when used as a bone substitute. Biomaterials 1993;14:403–406.
23. Walsh WR, Vizesi F, Michael D, Auld J, Langdown A, Oliver R, Yu Y, Irie H, Bruce W. Beta-TCP bone graft substitutes in a bilateral rabbit tibial defect model. Biomaterials 2008;29:266–271.
24. Mundy G, Garrett R, Harris S, Chan J, Chen D, Rossini G, Boyce B, Zhao M, Gutierrez G. Stimulation of bone formation in vitro and in rodents by statins. Science 1999;286:1946–1949.
25. Stein D, Lee Y, Schmid MJ, Killpack B, Genrich MA, Narayana N, Marx DB, Cullen DM, Reinhardt RA. Local simvastatin effects on mandibular bone growth and inflammation. J Periodontol 2005; 76:1861–1870.
26. Nyan M, Miyahara T, Noritake K, Hao J, Rodriguez R, Kuroda S, Kasugai S. Molecular and tissue responses in the healing of rat calvarial defects after local application of simvastatin combined with alpha tricalcium phosphate. J Biomed Mater Res B Appl Biomater 2010;93:65–73.
27. Boyne PJ, Salina S, Nakamura A, Audia F, Shabahang S. Bone regeneration using rhBMP-2 induction in hemimandibulectomy type defects of elderly sub-human primates. Cell Tissue Bank 2006;7:1–10.
28. Duan Z, Zheng Q, Guo X, Li C, Wu B, Wu W. Repair of rabbit femoral defects with a novel BMP2-derived oligopeptide P24. J Huazhong Univ Sci Technol Med Sci 2008;28:426–430.
29. Giannoudis PV. Fracture healing and bone regeneration: Autologous bone grafting or BMPs? Injury 2009;40:1243–1244.
30. Nyan M, Sato D, Kihara H, Machida T, Ohya K, Kasugai S. Effects of the combination with alpha-tricalcium phosphate and simvastatin on bone regeneration. Clin Oral Implants Res 2009;20:280–287.
31. Skoglund B, Aspenberg P. Locally applied Simvastatin improves fracture healing in mice. BMC Musculoskelet Disord 2007;8:98.
32. Hatano H, Maruo A, Bolander ME, Sarkar G. Statin stimulates bone morphogenetic protein-2, aggrecan, and type 2 collagen gene expression and proteoglycan synthesis in rat chondrocytes. J Orthop Sci 2003;8:842–848.
33. Sonobe M, Hattori K, Tomita N, Yoshikawa T, Aoki H, Takakura Y, Suguro T. Stimulatory effects of statins on bone marrow-derived mesenchymal stem cells. Study of a new therapeutic agent for fracture. Biomed Mater Eng 2005;15:261–267.
34. Zhang H, Lin C-Y. Simvastatin stimulates chondrogenic phenotype of intervertebral disc cells partially through BMP-2 pathway. Spine (Phila Pa 1976) 2008;33:525–531.
35. Zhang M, Li XP, Qiao Y, Nie SP, Ma CS. Does treatment with statins have the potential of enhancing vascular calcification? Chin Med J (Engl) 2008;121:473–474.
36. Mankani MH, Kuznetsov SA, Fowler B, Kingman A, Robey PG. In vivo bone formation by human bone marrow stromal cells: Effect of carrier particle size and shape. Biotechnol Bioeng 2001;72:96–107.
37. Sun JS, Tsuang YH, Chang WH, Li J, Liu HC, Lin FH. Effect of hydroxyapatite particle size on myoblasts and fibroblasts. Biomaterials 1997;18:683–690.

J Mater Sci: Mater Med (2011) 22:1489–1499
DOI 10.1007/s10856-011-4329-0

Enhanced osteoblast and osteoclast responses to a thin film sputtered hydroxyapatite coating

J. Hao · S. Kuroda · K. Ohya · S. Bartakova · H. Aoki · S. Kasugai

Received: 19 November 2010 / Accepted: 27 April 2011 / Published online: 13 May 2011

Abstract A sputtering technique followed by a low temperature hydrothermal treatment has been demonstrated to produce a dense-and-bioactive hydroxyapatite thin film coating. The purpose of the present study was to investigate osteoblast and osteoclast responses to the hydroxyapatite coated plates and titanium plates with similar roughness. Rat bone marrow stromal cells were cultured on these plates to induce osteoblasts. The cells showed a significantly enhanced proliferation on the hydroxyapatite surface, accompanied by increase of osteoblastic phenotypes. The co-cultured osteoclasts exhibited the significantly different cell number and morphology between the hydroxyapatite and the titanium surfaces. A series of osteoclast marker genes were more stimulated on the hydroxyapatite and thirty two percent of the hydroxyapatite surface area could be resorbed by osteoclasts. The thin film sputtered hydroxyapatite could provide a favorable surface for both osteoblast and osteoclast formation and their function, indicating its good osteoconductivity and biodegradability.

J. Hao · S. Kuroda (✉) · S. Kasugai
Section of Oral Implantology and Regenerative Dental Medicine, Tokyo Medical and Dental University, 1-5-45 Yushima, Bunkyo-ku, Tokyo 113-8510, Japan
e-mail: skuroda.mfc@tmd.ac.jp

J. Hao · S. Kasugai
Global Center of Excellence (GCOE), Tokyo Medical and Dental University, Tokyo, Japan

K. Ohya
Section of Pharmacology, Tokyo Medical and Dental University, Tokyo, Japan

S. Bartakova
Department of Prosthodontics, Masaryk University, Brno, Czech Republic

H. Aoki
International Apatite Institute Co, Tokyo, Japan

1 Introduction

Hydroxyapatite (HA), $Ca_{10}(PO_4)_6(OH)_2$, is a well-known bioceramic material for medical application because of its close similarity to the chemical and mineral components of teeth and bones. It has been used to provide bioactive coatings for orthopedic and dental implants [1]. As early as 1960s, the concept of biological fixation of load-bearing implants using HA coatings was proposed as an alternative to cemented fixation. It has been reported that HA coating could provide an excellent long-term success rate in a minimum 10 years follow-up study [2]. Furthermore, the HA coating degradation caused by osteoclastic resorption is considered to be the result of the similar function taking part in the bone remodeling as seen in any other part of the skeleton [3].

A number of methods have been developed to deposit HA coating including plasma spraying, Sol–Gel, pulsed laser deposition, ion-beam method and sputtering. Currently plasma spraying is the major commercially available technique for HA coating due to the high reproducibility and economic efficiency of the process [4, 5]. However, problems cited with the plasma sprayed HA coating include variation in bond strength between the coatings and metallic substrate, non-uniformity in coating density, poor adhesion between the coating and substrates, microcracks on the coating surface and poor resistance to delamination due to the coating process [4, 6]. Thereafter, as an alternative to the plasma spray method, a radio frequency magnetron sputtering technique has been

investigated [7]. The sputtering technique has advantages of depositing thin coatings (0.5–3 μm) with strong adhesion, compact microstructure and controlled elemental composition [8]. However, it has been reported that it is necessary to find an optimal heat treatment to inhibit the dissolution properties of the coating by crystallizing the film [9]. The conventional high temperature (≥600°C) heat treatment may result in the appearance of cracks in the coating because of the difference in the thermal expansion coefficient of Ca–P and metal substrate [7]. For this reason, it is necessary to crystallize the HA film at low temperature. Ozeki et al. reported a hydrothermal technique at as low as 110°C to crystallize sputtered amorphous HA film, and the film-to-substrate adhesion strength increased by over twofold. In vivo pullout tests, a 1.6 times higher bone-bonding strength was achieved by the hydrothermal technique than by the plasma spray method [10]. After the hydrothermal treatment, a surface morphology of needle-like HA crystal was observed by scanning electron microscopy. In addition, the proliferation and alkaline phosphatase (ALP) activity of MC3T3-E1 can be greatly improved by the hydrothermal treatment [11].

Bone is a dynamic tissue, and the long-term maintenance of osseointegration of implant requires a continuous remodeling of the bone-implant interface. Osteoclasts may play an important role in the initial period after implant placement or prepare the implant surface for the bone-forming activity of the osteoblasts [12]. Several investigators have examined the ability of osteoclasts to resorb various forms of calcium phosphate. Gomi et al. reported that osteoclasts form and are capable of resorbing sintered HA and that the rugosity of the HA increases the formation and resorptive activity of the osteoclasts [13]. In contrast, rabbit osteoclasts were found to resorb bone and sintered carbonate apatite but not sintered hydroxyapatite [14]. Those contradictory results might be due to the different sources of the osteoclasts and preparation of calcium phosphates as to crystal structure, grain size and surface roughness [12]. So far, there is no report regarding the osteoclast response to sputtered HA surface.

In the present study, the rat bone marrow stromal cell culture system was used to induce osteoblasts and a co-culture system of primary mouse calvarial osteoblasts and bone marrow cells was performed to entice osteoclast differentiation. And then both osteoblast and osteoclast formation and their function on the surface of the sputtered HA coating were compared to those on rough titanium surface by examining cell proliferation, gene expression and cellular morphological organization. Furthermore, HA coating degradation was also evaluated. The main aim of the present study was to investigate whether the sputtered HA coating would behave in more favorable a manner than non-coated surface-modified titanium substrates.

2 Materials and methods

2.1 Preparation of sputtered HA film on titanium plates

Commercially available grade 2 pure titanium plates ($20 \times 20 \times 1$ mm^3) were used as substrates. Titanium plates coated with or without sputtered HA were manufactured with similar surface roughness. Briefly, all the titanium plates were sandblasted by fluorapatite crystal and then subjected to an acid etching treatment. RF magnetron sputtering was carried out on half of these plates using an SPF-410H (ANELVA Corp.) chamber to produce a HA film with an average thickness of 1.1 μm. Subsequently, a hydrothermal treatment was performed at a temperature of 120°C in an electrolyte solution containing calcium and phosphate ions for 20 h. The composition of the solution was described in detail in the previous study [10]. All samples were sterilized in an autoclave at 121°C for 28 min and packed in polypropylene bags separately. Surface observation and elemental analysis were carried out using scanning electron microscopy (SEM) (JSM-5310LV, JOEL, Tokyo, Japan) and energy dispersive X-ray spectroscopy (EDS) (EMAX-7000, Horiba Ltd., Kyoto). The X-ray diffractometry pattern (XRD) was identified by RINT1400 (Rigaku Corp., Japan) using a CuKα radiation source operating at 50 kV and 100 mA excitation current. The surface roughness (Ra) was determined using a surface measurement tester (SURFCOM 130A).

2.2 Osteoblastic cell culture

Rat bone marrow cells were prepared according to the method of Maniatopoulos et al. [15]. Briefly, rat bone marrow cells isolated from the femora of 5 week-old male Wistar rats were cultured on these plates placed in 6-well culture dishes at a cell density of 10^6 cells/cm^2, maintained in α-MEM with 10% fetal bovine serum at 37°C in a humidified atmosphere consisting of 95% air and 5% CO_2. After 24 h, the medium was removed and changed to fresh one supplemented with osteogenic reagents (50 μg/ml ascorbic acid, 10 mM β-glycerophosphate, 10 nM dexamethasone). The culture medium was changed every 2 days.

2.3 Cell attachment and proliferation

After 24 and 72 h incubation, the culture medium was removed and the wells were washed three times with phosphate buffered saline (PBS) to eliminate unattached cells. The adherent bone marrow stromal cells were fixed and stained using fluorescent dyes, DAPI (molecular probes, Invitrogen, USA), and observed under a fluorescence microscope (Biozero BZ-8000, Keyence). In

addition, the proliferative activity of the cells was measured by BrdU incorporation during DNA synthesis. At day 2 of culture, BrdU reagent with the final concentration of 10 μM (Roche Applied Science, Mannheim, Germany) was added to the culture wells and incubated for 10 h at 37°C. After the labeling process, the cells were fixed and incubated with anti-BrdU-peroxidase working solution for 90 min. After washing, substrate solution (tetramethylbenzidine) followed by stop solution was added until color development was sufficient for photometric detection. Absorbance at 450 nm was measured using Wallace 1420 ARVOsx multi-label counter.

2.4 Measurement of DNA amount and ALP activity

Cells were washed with PBS, scraped, lysed by 0.1% Triton X100 (Sigma, St. Louis, MO, USA), and sonicated to destroy cell membranes. After centrifugation at 15,000 rpm for 10 min at 4°C, 200 μl of the supernatant was extracted from each sample and assayed for ALP activity and DNA content measurements. To determine DNA content, 100 μl of the prepared supernatant of each sample was mixed with 100 μl of 1 μg/ml Hoechst 33342 dye in the wells of a 96-well plate and processed with a fluorescent DNA quantification kit (Bio-Rad Laboratories, Hercules, CA, USA). The samples were then measured with the Wallace 1420 ARVOsx multi-label counter at excitation and emission wavelengths of 365 and 460 nm, respectively. Subsequently, to assess the quantitative and kinetic determination of ALP activity, 50 μl of the supernatant of each sample was added to 100 μl working solution (*p*-nitrophenyl phosphate solution) in the wells of another 96-well plate. The reaction was measured with the multi-label counter at a wavelength of 405 nm. ALP activity was normalized by total DNA amount of each sample.

2.5 Mineralization assay

The mineralization capability of cultured osteoblasts was examined at days 7 and 21. The cells were fixed with methanol and stained with Alizarin Red. The area of mineralized nodules of each sample was measured using a computer image analyzer (Image J, National Institute of Health, USA). To eliminate non-specific binding of Alizarin Red Stain, nodules bigger than 0.2 mm^2 were calculated. The result is represented as percentages of Alizarin Red positive area over total culture area.

2.6 Osteoclastic cell culture

Osteoclasts generated by a co-culture system [16] were also cultured on these titanium plates inserted in 6-well culture dishes. Briefly, osteoblast (3×10^5 cells/well) obtained by sequential collagenase digestion of newborn mouse calvariae and bone marrow cells (3×10^6 cells/well) obtained from femora and tibiae of 6 week-old male ICR mice were co-cultured in the normal medium (α-MEM, 10% fetal bovine serum) supplemented with 10^{-8} M 1,25-$(OH)_2$-vitamin D_3 and 10^{-6} M prostaglandin E_2. For osteoclast morphology and function assays, the co-culture was also performed on ivory dentine slices and polystyrene culture wells as control.

2.7 Osteoclast number and morphology

After 4, 5 and 7 days co-culture, cells were fixed with 3.7% formaldehyde in PBS for 10 min and washed three times with PBS and permeabilized with 0.1% Triton X-100 in PBS for 5 min. The cells were rinsed three times with PBS and treated with 1% bovine serum albumin for 10 min. Cells were stained using fluorescent dyes, 5 units/ml Alexa 488 phalloidin (actin green color, Molecular Probes, Invitrogen, USA) and 300 nM DAPI (nuclei blue color, Molecular Probes, Invitrogen, USA). Subsequently, tartrate-resistant acid phosphatase (TRAP) staining was also performed. In brief, cells were rinsed with ethanol–acetone solution (50:50, v/v) for 1 min, and stained with TRAP solution for 10 min at room temperature. To prepare TRAP solution, 5 mg of naphthol AS-MX phosphate (Sigma, USA) was diluted in 0.5 ml of *N*,*N*-dimethylformamide (Wako, Japan) and this solution was combined with 30 mg of fast red violet LB salt (Sigma, USA) and 50 ml of 0.1 M sodium acetate buffer (pH 5.9) containing 50 mM sodium tartrate. TRAP positive cells with three or more nuclei were considered as osteoclasts. TRAP positive cells and cellular structures such as actin and multi-nuclei were visualized using a fluorescence microscope (Biozero BZ-8000, Keyence). The osteoclast number, area, perimeter and Feret's diameter were quantified by an image analyzer (Image J, National Institute of Health, USA).

2.8 HA coating degradation

At osteoclast culture day 7, the HA samples were soaked in 1 M ammonia, and the cells were removed by sonicating for 1 min. To analyze the HA coating degradation, element distribution of the HA coating was performed by energy dispersive X-ray mapping. The HA coated samples immersed in the same culture medium for 7 days were used as control. The coating degradation area was calculated by Image J.

2.9 RNA isolation and real-time quantitative RT-PCR

Cells in both culture systems were lysed in TRIzol Reagent (Invitrogen, USA) and total RNA was precipitated in

isopropanol. First-strand cDNA was reverse-transcribed from total RNA with SuperScript™ IIIFirst-Strand Synthesis System for RT-PCR (Invitrogen, USA). The expression levels of osteoblast or osteoclast related genes were determined using the real-time quantitative reverse transcription-polymerase chain reaction (RT-PCR). SYBR Green-based real-time PCR analysis was carried out with the ABI Prism 7,300 Sequence Detection System (Applied Biosystems, Foster City, CA, USA). Expression levels were determined using the relative threshold cycle (C_T) method as described by the manufacturer of the detection system. Expression levels were stated in terms of fold increase or decrease relative to that of Ti group at the first time point. This was calculated for each gene by evaluating the expression $2^{-\Delta\Delta CT}$, where $\Delta\Delta$CT is the result of subtracting $[C_{T\ gene}-C_{T\ GAPDH}]_{(Ti\ calibrator)}$ from $[C_{Tgene}-C_{TGAPDH}]_{(HA\ group)}$. The primers used are shown in Table 1.

2.10 Statistical analysis

All experiments were performed in duplicate, and results were calculated as mean ± SD. Statistical analysis was performed by the statistic software 11.5 SPSS for Windows. ANOVA with Scheffe test was used for comparing the significance among groups at each time point. *t*-Test was used to determine the differences between the HA and Ti groups if data were available at only one time point. *P* values of less than 0.05 were considered to be statistically significant.

3 Results

3.1 The observations and characterizations of sputtered HA coating

Fig. 1a showed the XRD pattern of sputtered HA coating. The dotted lines and solid lines indicated the peaks of Ti and crystallized HA, respectively. EDS analysis confirmed the purity of the Ti (Fig. 1b) and the sputtered HA coating (Fig. 1c). The Ra values of the Ti and sputtered Ha coating were 1.25 ± 0.26 and 1.13 ± 0.39 μm, respectively. The Ca/P molar ratio was 1.70 ± 0.13 (Table 2).

Table 1 Real time RT-PCR primers

Gene	Sequence	Base pair	Sequence reference
Mouse GAPDH	(F) 5′ -CTCCCACTCTTCCACCTTCG-3′	99	NM008084
	(R) 5′-TTGCTGTAGCCGTATTCATT-3′		
Mouse TRAP	(F) 5′-TACCTGTGTGGACATGACC-3′	151	BC029644
	(R) 5′-CAGATCCATAGTGAAACCGC-3′		
Mouse v-ATPase	(F) 5′-TCCAACACAGCCTCCTACTT-3′	161	AB022322
	(R) 5′-ACAGCAAAGGCAGCAAAC-3′		
Mouse CTR	(F) 5′-TCAGGAACCACGGAATCCTC-3′	101	NM007588
	(R) 5′-ACATTCAAGCGGATGCGTCT-3′		
Mouse CathepsinK	(F) 5′-TGTATAACGCCACGGCAAA-3′	195	X94444
	(R) 5′-GGTTCACATTATCACGGTCACA-3′		
Mouse MMP-9	(F) 5′-TCCAGTACCAAGACAAAG-3′	183	X72795
	(R) 5′-TTGCACTGCACGGTTGAA-3′		
Mouse RANKL	(F) 5′-ACCAGCATCAAAATCCCAAG-3′	203	AB008426
	(R) 5′-TTGAAAGCCCCAAAGTACGT-3′		
Rat GAPDH	(F) 5′-AACTCCCATTCTTCCACCTT-3′	200	M17701.1
	(R) 5′-TCTCGTTCTCTCTCCGGGA-3′		
Rat TGF-β1	(F) 5′-CAACAATTCCTGGCGTTACC-3′	200	NM_021578.2
	(R) 5′-TTAGTTACCCTAGTCAGGGT-3′		
Rat ALP	(F) 5′-GTCACAGCCAGTCCCTCAAC-3′	202	NM_013059.1
	(R) 5′-GCTGAGGGGACAAACCTTAT-3′		
Rat Col1	(F) 5′-TTGACCCTAACCAAGGATGC-3′	197	NM_053356.1
	(R) 5′-TTATGTTGCGTCTTCCCCAC-3′		
Rat Runx2	(F) 5′-GCCAGGTTCAACGATCTGAG-3′	201	NM_053470.1
	(R) 5′-CAAACAAGAGACTGGCGGAG-3′		
Rat osteocalcin	(F) 5′-AGCTCAACCCCAATTGTGAC-3′	190	M11777
	(R) 5′-TTTCATACCTGCCGTGTCGA-3′		

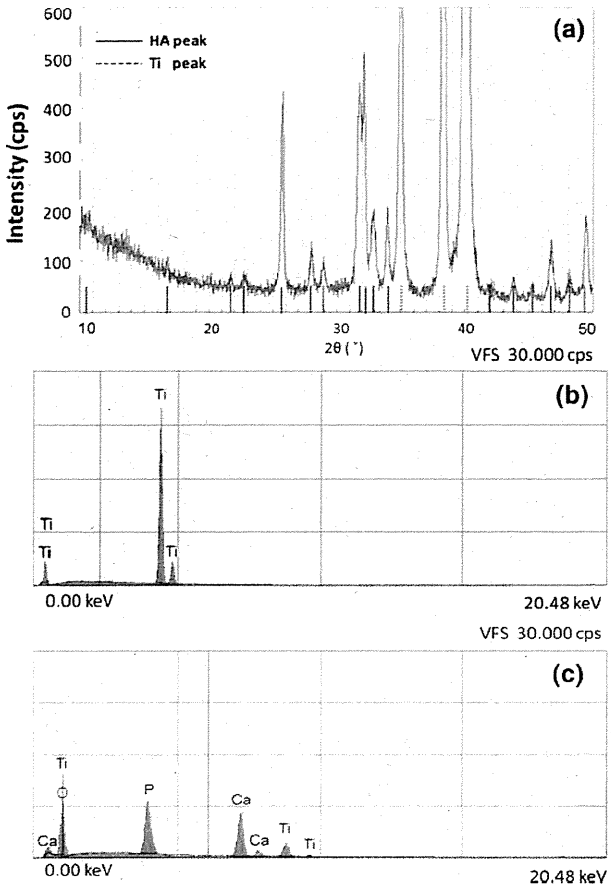

Fig. 1 X-ray diffractometry (XRD) pattern of the sputtered HA film (**a**). Energy dispersive X-ray spectroscopy (EDS) spectrum of the Ti plate (**b**) and the sputtered HA coated Ti plate (**c**)

3.2 Enhanced attachment and proliferation of bone marrow stromal cells on sputtered HA surface

Cell density was consistently greater on the sputtered HA surfaces (Fig. 2b, d) than that on Ti surfaces (Fig. 2a, c) at days 1 and 3. The proliferation determined by BrdU incorporation also showed a significantly higher level on the sputtered HA surface compared with Ti surfaces, confirming increased cell proliferation (Fig. 2e).

3.3 Enhanced osteoblastic phenotypes on sputtered HA surface

ALP activity was measured on days 3, 7 and 14. In both groups, ALP activity increased time dependently. In detail, ALP activity was showing the same level on both surfaces at day 3; however, cells on sputtered HA at days 7 and 14 accelerated ALP activity at a significant higher level compared with those of the Ti group (Fig. 3a).

In addition, the area of mineralized nodule detected by Alizarin Red stain was also greater on HA surface. At day 7, the HA group showed a 4.3 fold increase in nodule formation compared to the Ti group ($P < 0.01$). Until day 21, the HA group still exhibited a higher level of nodule formation than the Ti group ($P < 0.05$) (Fig. 3b). Real-time PCR demonstrated mRNA expressions of osteoblastic marker genes of interest as fold changes to the control level. Rat mRNA expression levels of ALP and TGF-β were significantly increased on HA surface by day 7 ($P < 0.05$). However, the other genes including osteocalcin, collagen type I and runx2 showed significant increases only at day 14 ($P < 0.05$) (Fig. 3c–g).

Table 2 Surface roughness and Ca/P ratio. ($n = 3$)

Sample	Ra (μm)	Ca/P
Ti	1.25 ± 0.26	
HA	1.13 ± 0.39	1.70 ± 0.13

3.4 Osteoclast formation and morphometry

TRAP positive cells were observed in all experimental groups as early as day 4 of the co-culture. The fluorescence microscopy images of actin structures of these multinucleated cells overlapped with the TRAP staining (Fig. 4a–h).

Osteoclasts could form on several substrates and then exhibit different actin structures. Phalloidin fluorescence staining showed that the actin ring sizes were increasing from day 4 to day 7. Moreover, the actin ring structure on the sputtered HA surface was consistently showing smaller size compared to that on the Ti surface and the polystyrene culture well, but almost the equal size to that on dentine slice (control > Ti > HA ≈ dentine) (Fig. 5a–c). Osteoclasts on Ti and polystyrene surface were exhibiting typical podosome belts with loose actin network by small actin dots, also called actin cloud (Fig. 4e, g). In contrast, the osteoclasts on both HA and dentine were able to acquire a sealing zone, represented by a dense band of actin (Fig. 4a, c).

As shown in Fig. 5d, the number of osteoclasts on the dentine or HA was larger than those on Ti and the control surfaces throughout the culture period ($P < 0.01$). Significant difference of TRAP positive cell number between the dentin and the HA groups was found only at day 4 ($P < 0.01$) but not at days 5 and 7.

3.5 Osteoclast function and HA coating degradation

To further confirm the functionality of the osteoclasts, the mRNA levels of a series of their growth and differentiation markers including receptor activator of nuclear factor kappa B ligand (RANKL), osteoprotegerin (OPG), TRAP,

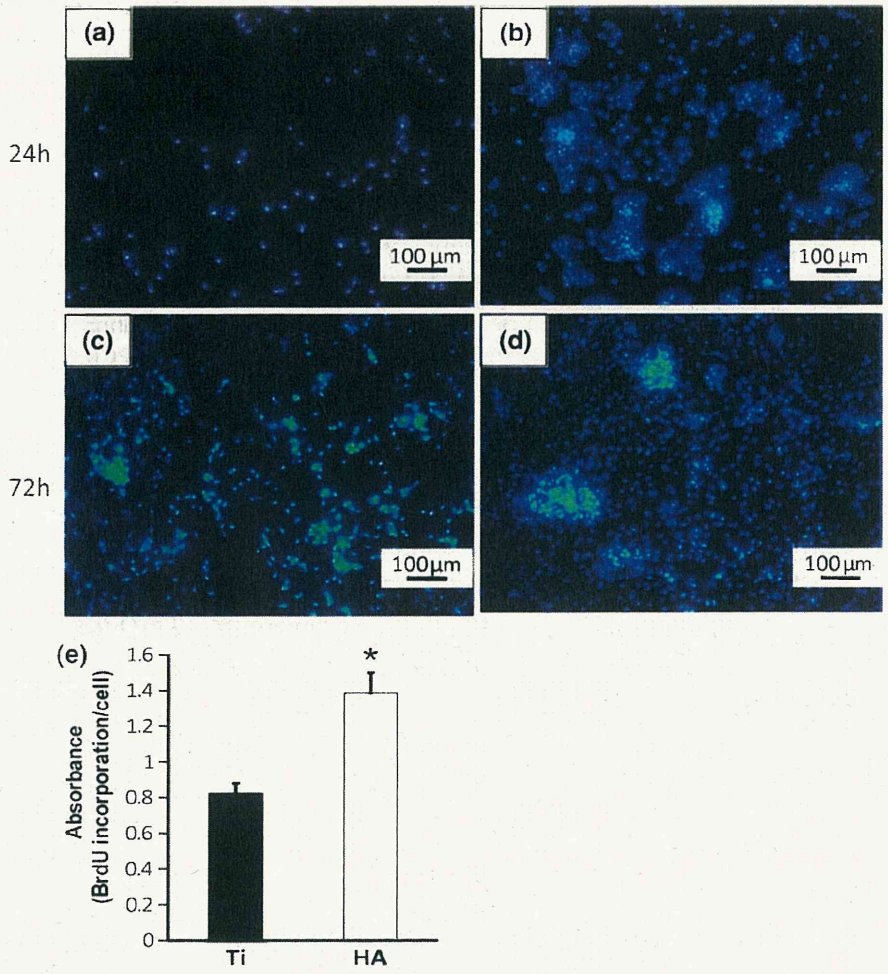

Fig. 2 Initial behavior of bone marrow stromal cells on the Ti and the HA surfaces. DAPI staining of bone marrow cells attached to the Ti (**a**, **c**) and the HA (**b**, **d**) after 24 h (**a**, **b**) and 72 h (**c**, **d**) incubation. The cell proliferation was determined by BrdU incorporation and the absorbance measurement at 450 nm (**e**). And each column represents values as the mean ± SD ($n = 6$). *Statistically different between HA and Ti groups ($P < 0.05$)

vacuolar-type H-ATPase (v-ATPase), calcitonin receptor (CTR), cathepsin K, and MMP-9 were analyzed by quantitative real-time RT-PCR. V-ATPase and the ratio of RANKL/OPG mRNA expression were significantly increased on HA than on Ti at day 5 and so were TRAP and CTR transcription at day 7. However, no differences could be observed in terms of Cathepsin K and MMP-9 expression (Fig. 6a–h).

After 7 days of culture, cells were removed from the samples and the coating degradation was analyzed by energy dispersive X-ray mapping. The elemental distribution of calcium, phosphorus and titanium was shown in Fig. 7. The regions with HA degradation were indicated with arrows in Fig. 7a–d, where, Ca and P were completely absent. In addition, these regions were rich in Ti which indicated the degradation of the HA coating and the titanium substrate exposure. However, in the control group, no coating degradation was observed after soaking in the same culture medium for 7 days. Ca and P were homogeneously distributed throughout the HA coating, and Ti could be hardly detected (Fig. 7e–h). These results suggested that the coating degradation were mediated by osteoclastic functional resorption but not HA chemical dissolution. The osteoclastic degradation occurred in 32.3 ± 3.5% of the sputtered HA coating.

4 Discussion

In this study, a rat bone marrow stromal cell culture was performed to evaluate the osteoblast response on the HA coated titanium. One advantage of cell culture systems is that it can focus on a part of the physiological condition, wherein interaction among the cells and signal molecules can be clarified. Since the implant materials directly contact bone marrow cells after implantation, it is advantageous to use a culture system to investigate implant materials as substrates for the cells [17]. The cell density was consistently greater on the sputtered HA surface than the Ti surface on days 1 and 3 of culture, wherein, by day 3, the cells had appeared to reach confluence on the HA surface but not on the Ti surface. Notably, this increment of